Self-organization of isotropic droplets in smectic-*C* free-standing films

C. Völtz* and R. Stannarius
Otto-von-Guericke-Universität Magdeburg, Institut für Experimentelle Physik, D-39106 Magdeburg, Germany
(Received 18 June 2004; published 2 December 2004)

Free standing smectic films have been investigated at the transition from the smectic-*C* phase to the isotropic phase. In the vicinity of the bulk transition temperatures, isotropic droplets of micrometer size appear in the film. Such systems represent convenient models for anisotropic, two-dimensional emulsions. A characteristic feature of the droplets is their mutual interaction by elastic distortions of the local orientation of the film, the *c* director, which are related to the anchoring conditions of the *c* director at the droplet border. We describe in detail the director deformations created by isotropic droplets of different sizes, and their role in the spontaneous organization of regular droplet patterns. Depending upon droplet size and anchoring strength, topological defects can be induced in the *c*-director field. Qualitative differences to literature data on cholesteric droplets in smectic-*C** films are discussed.

DOI: 10.1103/PhysRevE.70.061702 PACS number(s): 64.70.Md, 61.30.Gd, 61.30.−v, 42.70.Df

I. INTRODUCTION

Isotropic particles dispersed in liquid crystals have recently attracted increasing attention for their unique collective behavior leading to a rich variety of unusual colloidal structures [1]. In particular, isotropic (oil, water, or liquid crystal) droplets in nematic bulk phases [2–4] and droplets in smectic films [5–16] have been extensively investigated. Compared to isotropic dispersions, interactions mediated by the director field lead to qualitatively new phenomena in these systems. In nematic bulk phases, the director field is three dimensional. Droplets and defects form topological dipoles, which interact by the director field deformations, as has been shown in models for nematic phases [17–19]. In the smectic free standing films, one deals essentially with a two dimensional director field. Whereas in nematics, the directions $\vec{n}$ and $-\vec{n}$ are equivalent, the *c* director in smectic-*C* (Sm-*C*) films describes the tilt azimuth and is a vector. These two principal differences have to be kept in mind when in the following, director structures and droplet interactions are discussed.

The investigation of the formation and dynamics of isotropic droplets in smectic-*A* (Sm-*A*) free-standing films [5–7] has shown that the droplets have the shape of flat lenses. In Sm-*A* films of uniform thickness, the droplets are force free and do not interact with each other. They are randomly distributed in the film plane under isothermal conditions.

As well as Sm-*A*, mesogens in the Sm-*C* phase can form thin films, freely suspended across a supporting frame [20]. Such films consist of an integer number of molecular layers in the plane of the film. In Sm-*C*, each layer can be considered as a two-dimensional anisotropic liquid, with the rodlike molecules tilted in a preferential direction. The average orientation of the long molecular axes forms the tilt angle θ with the smectic layer normal. The in-plane orientation of the tilt in the smectic layers is described by the so-called *c* director, defining the tilt azimuth [10].

Droplet formation at the smectic-*C**–cholesteric transition has been studied earlier. It has been shown that in the material investigated in Ref. [11], each droplet is accompanied by an $S=-1$ defect. Strong radial anchoring of the *c* director at the droplet boundaries has been assumed there. Similar to the situation in nematics, the $S=-1$ defect appears detached from the droplet in the anisotropic phase. Together with the droplet, that can be considered as an $S=+1$ defect in the *c*-director field, it forms a a topological dipole. The formation and stability of such dipoles in the general case of a disklike inclusion in a smectic-*C* film has been discussed theoretically in detail in Ref. [21]. Chaining and the formation of droplet lattices have been reported [13–15]. For azo-dye doped systems [12], it has been demonstrated that light illumination can create droplets on Sm-*C** films. But so far, the director fields and interactions have not been analyzed in detail.

We investigate isotropic droplets produced by heating (nonchiral) Sm-*C* films to the bulk Sm-*C*–isotropic transition temperature. Like in the smectic-nematic and smectic-cholesteric systems, a characteristic feature of the droplets is their spontaneous chaining in the *c*-director field and the formation of short-range-ordered lattices. The droplets interact with each other by the distortions of the *c*-director field. These rather general observations are in accordance with those reported in Refs. [11,12]. However, we will demonstrate that the material investigated here forms director structures of qualitatively different types than those reported for the Sm-*C** films. Of primary interest in this study is the qualitative understanding of the director deformations that lead to self-organization (see Fig. 1). Therefore we focus particularly on large droplets, which offer the opportunity to resolve textures details. We find defect-free textures as well as textures with half integer defect pairs lying on the smectic-isotropic interface of the droplets, but no isolated integer strength defects have been found in our experiments. A model will be presented that classifies these different textures qualitatively by the ratio of the droplet radius and a characteristic length ξ_0, which depends on elastic constants and surface anchoring strength of the *c* director. In addition, a photosensitive compound (azoxybenzene-derivative) has

*Email address: camilla.voeltz@physik.uni-magdeburg.de

FIG. 1. (Color online) Chains of isotropic droplets in a smectic film (approximately 300-nm film thickness) of the material 11OAB, observed in unpolarized white light near the clearing point, droplet diameters in the range of 2–5 μm.

been investigated, where droplet formation can be initiated by light illumination, also in the Sm-*C* phase. In contrast to the dye-doped system studied in Ref. [12], our material is a pure substance.

The paper is organized as follows. In Sec. II, the experimental setup is described and in Sec. III, the theoretical model of the director configurations around isotropic droplets in free standing films is introduced. In Sec. IV, the experimental results are presented and discussed. We start with the description of the director deformations around isolated single droplets and the origin of the defects. Then, we discuss the director fields around pairs of droplets, and we describe the self-organization to droplet chains and lattices. The last section contains the summary and conclusions.

II. EXPERIMENTAL SETUP

The chemical structures of the compounds SF20 and 11OAB (4,4′-bis-*n*-undecyloxy-azoxybenzene) studied here are shown in Fig. 2. The substance SF20 has the phase sequence: Cryst. $\overset{85\ °C}{\leftrightarrow}$ Sm-C_{ac} $\overset{93\ °C}{\leftrightarrow}$ Sm-C_{sc} $\overset{102\ °C}{\leftrightarrow}$ isotropic, where ac stands for anticlinic (alternating tilt between the layers) and sc for synclinic (same tilt azimuth in adjacent layers) Sm-*C* phases. The substance 11OAB has the phase sequence: Cryst. $\overset{80.8\ °C}{\leftrightarrow}$ Sm-*C* $\overset{121.4\ °C}{\leftrightarrow}$ isotropic.

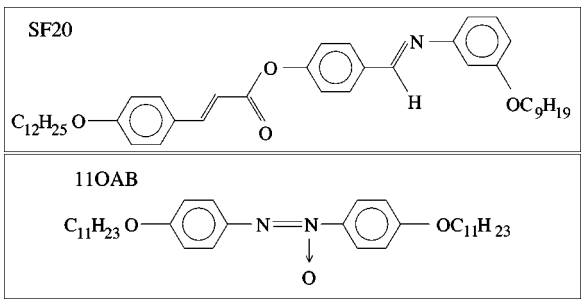

FIG. 2. Chemical structure of the mesogenic materials.

Films are prepared by drawing a small amount of liquid crystal in the Sm-*C* state across a hole of radius $R=1$ mm in a support plate. The support of the film is temperature controlled with a commercial heating stage (Linkam THMS600) with a temperature stability of 0.1 K. However, we note that the intense illumination of the film has a measurable influence on the film temperature, so that the absolute stability of the temperature is estimated to be accurate to ±0.5 K only.

The textures are in general observed between crossed polarizers with an optical microscope (Zeiss Axioskop 40) in reflection mode. In some of the experiments, the polarizers are slightly decrossed to obtain additional information on the director field. Images of the film texture are taken with a charge-coupled device camera connected to a computer and processed digitally. Experiments where the thickness profile of the films/droplets is of interest are performed in monochromatic light, a metal interference filter (590 nm) replaces the analyzer there. The thickness of all films is in the range of 100–200 smectic layers.

III. THEORETICAL MODEL

The structure and shape of the isotropic droplets has been analyzed in detail for Sm-*A* films; it is related to surface and interface tensions of the material [5–7]. The shapes of isotropic droplets in Sm-*C* films is essentially similar, and as in the Sm-*A* films, the droplets interact with film thickness gradients by capillary forces. We concentrate here only on the differences to the Sm-*A* films, which originate from the existence of a *c*-director field in the Sm-*C* film surrounding the droplet.

The elastic free energy f_e per volume for a thin planar film has the form (e.g., Refs. [22,23])

$$f_e = \frac{1}{2}K_S(\vec{\nabla}\cdot\vec{c})^2 + \frac{1}{2}K_B(\vec{\nabla}\times\vec{c})^2 \tag{1}$$

in which K_S and K_B are the splay and bend curvature elastic constants for the *c* director. We assume here that $\vec{c}$ varies only in the film plane but is uniform along the film normal. The constants K_S and K_B are in general not equal, but we will assume $K_S=K_B=K$ in one-constant approximation for the following *qualitative* analysis. The alignment of the *c* director by the smectic-isotropic interface of the droplet border is considered by an anchoring energy W_0, which results in a free energy contribution per interface area

$$f_0 = W_0(\vec{c}\cdot\vec{n})^2, \tag{2}$$

where $\vec{n}$ is the direction normal to the interface. A characteristic length ξ_0 describing the ratio of anchoring strength and volume elasticity can be defined by

$$\xi_0 = \frac{K}{W_0}. \tag{3}$$

It can roughly be assigned to a length, over which a director distortion induced by the surface extends into the film. When we analyze isotropic droplets of radius *r* in the smectic film, the ratio r/ξ_0 reflects the strength of the deformation of the director field created by the droplet in its surrounding, it

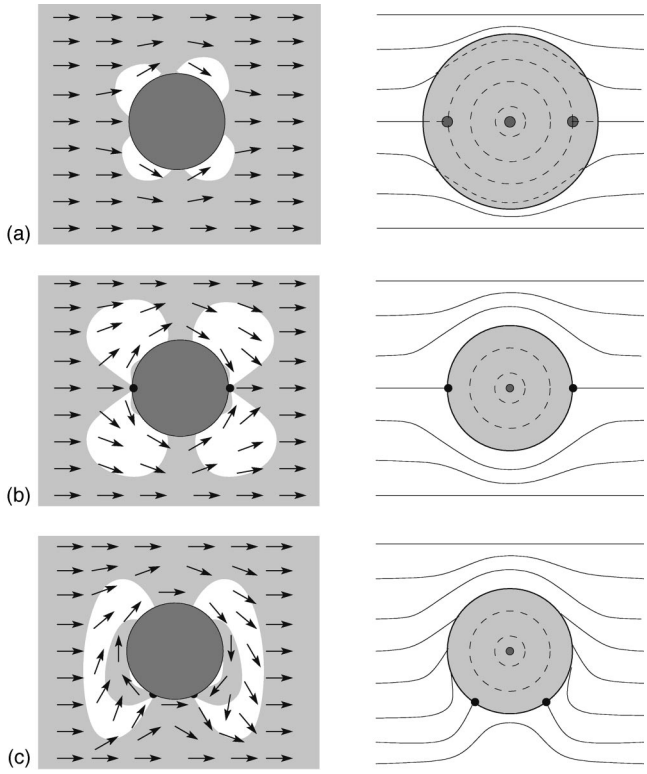

FIG. 3. Location of defects for increasing r/ξ_0. Images in the right column sketch streamlines of the field, images in the left column sketch the actual deformation. The grey shades symbolize the optical texture at crossed vertical/horizontal polarizers. (a) weak deformation, the three virtual defects are located well within the isotropic region inside the droplet, (b) the defect pair has reached the droplet border, the *c* director is tangential everywhere on the droplet border, and (c) the defects on the border approach each other, without coalescing.

characterizes the director field qualitatively: If $r \ll \xi_0$ (the anchoring energy term W_0 is very small), the director field is only weakly influenced near the surface of the droplet. It will be shown in the experimental section that in this case, the director field is in general defect free. The "streamlines" of the *c* director are qualitatively similar to those of a constellation of three virtual defects, a central $S=1$ and two lateral $S=-1/2$ defects in opposition (see Fig. 3). The first one is located in the droplet center. Of course, the latter two cannot be located in the Sm-*C* film either, because half integer defects are prohibited for the *c* director. They appear either in the form of virtual defects, located within the isotropic droplet area [Fig. 3(a)], or they lie exactly at the droplet boundary [Fig. 3(b)]. Since the director field in the vicinity of a freshly emerging small droplet is in general locally uniform and defect free, all droplets start with the topology of Fig. 3(a). With growing droplet radius *r*, the length of the interface increases, and consequently the influence of the anchoring conditions becomes stronger. Within our qualitative model, this is reflected in a growth of the distances between the virtual defects. Finally, with increasing influence of the boundaries (i.e., increasing r/ξ_0), the virtual half integer defect pair reaches the droplet border, as is illustrated in Fig. 3(b). The anchoring of the *c* director is then almost tangential. We note that in this situation, where three defects are lined up symmetrically to the droplet center, the director field does not have a dipolar structure as in nematics or in the smectic films studied earlier [10,17], but a dominatingly quadrupolar character. The four directions along the diagonals are equivalent in this configuration.

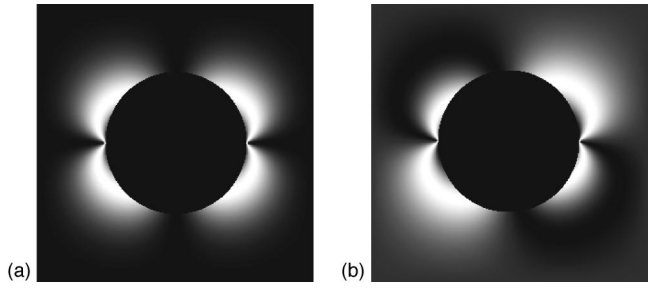

FIG. 4. Optical reflection image for $\xi_0=0$, director configuration as in Fig. 3(b); crossed polarizers along the horizontal and vertical directions (a) and rotated both by 10° (b).

The two half integer defects are trapped at the droplet border, they can shift along that border, but they cannot detach and leave into the Sm-*C* film. Usually, they gather on one side of the droplet [Fig. 3(c)]. When this occurs, the director configuration adopts dipolar character. The topological dipole is formed by the two half integer defects together with the virtual $S=1$ defect inside the droplet. We will show later that this symmetry change has important consequences for the self-organization and the alignment of droplet chains.

A detached $S=-1$ defect could only form if the two $S=-1/2$ defects combine on the droplet boundary. However, since these two defects repel each other, this scenario is rather exceptional. It would lead to a situation analogous to that observed by Cluzeau [10] (for radial director anchoring). However, we have not found examples of such configurations in our films.

For a quantitative calculation of the director configurations and elastic interactions, numerical calculations are being performed. Figure 4 shows the calculated texture of the director configuration depicted in Fig. 3(b). The polarizers have been assumed along the vertical and horizontal axes (a) and rotated by 10° (b). In the calculation, the *c* director $\vec{c}=(c_x,c_y)$ has been kept exactly tangential along the droplet border (corresponding to strong anchoring, $\xi_0 \to 0$), symmetries have been considered, and the director field has been determined by a relaxation method where both elastic constants have been set equal. The reflectivity is proportional to $c_x^2 c_y^2$.

The self-organization of the droplets in the film is a consequence of their interaction via the induced director deflections. There is an attractive force between droplets in a defect-free environment which may lead to pair formation as sketched in Fig. 5(a). Because of the symmetry of this configuration, one expects a preferential formation of chains diagonal to the *c* director, or of square lattices.

Droplets with two half-integer surface defects experience two interaction effects. First, they tend to rotate their defect pair into a common orientation. Second, they line up to pairs and chains as sketched in Fig. 5(b). They tend to distort the *c*

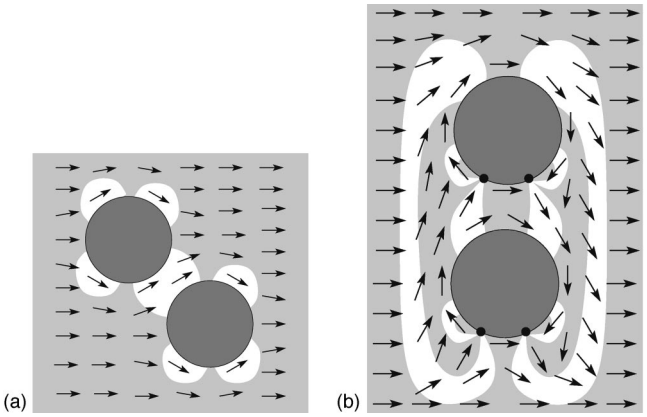

FIG. 5. (a) Two droplets with quadrupolar interactions of a defect-free director field, the droplets share one of the deflected "lobes." The droplet interconnection vector is diagonal to the (distant) undistorted director field. (b) Situation for two droplets with dipolar director configurations. It is difficult to make a definite statement about the alignment of this pair in the embedding director field.

director to an antiparallel orientation on both sides of the pair/chain.

IV. EXPERIMENTAL RESULTS

Observations of the film texture between crossed polarizers reveal details of the particular distortions of the *c*-director field around the particles, depending of the ratio $K/(W_0 \cdot r)$. The different textures actually observed are discussed in detail below. Before dealing with interactions of droplets, we analyze the distortions induced around individual droplets. We have selected examples of particularly large droplets where the director deflections are clearly resolvable.

A. Single small droplets

Qualitatively different configurations of the director field induced by single droplets on a Sm-*C* film are depicted and interpreted in the following images. If not otherwise stated, crossed polarizers are horizontal and vertical, respectively, and dark domains in the images correspond to *c*-director orientations parallel or antiparallel to the polarizers. Bright domains reflect diagonal orientations of the *c* director. With slightly decrossed polarizers or by insertion of a phase plate, one can assign an individual region to left or right inclined deflection. However, our observation technique is insensitive to the sign of the *c* director. The optical analysis of the images yields a consistent *c*-director field, but if all arrows are reversed, the resulting optical texture would be the same. We have established by a conoscopic observation method that the *c* director in our materials anchors preferentially tangential at the smectic-isotropic interface $(W_0 > 0)$, as well as at layer steps of the film.

Figure 6(a) depicts an experimental situation corresponding qualitatively to Fig. 3(a). The *c*-director field is deflected towards a tangential anchoring along the droplet interface, but is not strictly tangential yet. However, the deformation is already close to that of Fig. 3(b). The texture has approximately quadrupolar symmetry.

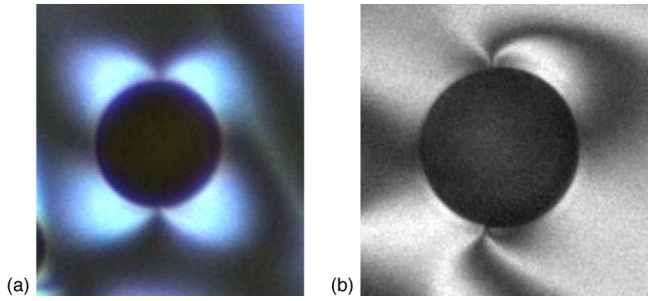

FIG. 6. Single droplets, SF20, $T = 101\ ^\circ$C. Polarizers are crossed along the vertical and horizontal, resp., in the images. (a) Defect free droplet, close to the defect formation, diameter 24.8 μm, and (b) droplet of 36.0 μm diameter, with two half integer surface defects in opposition. Note the qualitative agreement with Fig. 4.

The image shows a certain advantage of isotropic droplets compared to nematic or cholesteric inclusions: because of their optical isotropy, the black disk of the droplet area can clearly be discriminated from the surrounding smectic film, and a sharp droplet border is well defined.

With growing r/ξ_0, the increasing influence of the smectic-isotropic interface induces the pair of half-integer surface defects at the droplet border, as is seen in Figs. 6(b) and 7. The defect topology (the two $S = -1/2$ surface defects plus the virtual $S = 1$ defect in the droplet area) has a dipolar character in the latter. These images resemble the situations in Figs. 3(b) and 3(c), respectively.

We note that droplets with the geometry of Fig. 3(b) are observed only scarcely, while those with geometries of Figs. 3(a) and 3(c) are the rule. This may suggest that the configuration of Fig. 3(b) is not stable, but the defect pair, once created at the droplet border, gathers on one side of the droplet.

B. Huge droplets

When the droplets grow further, the director field becomes more complex, and moreover, the droplets develop

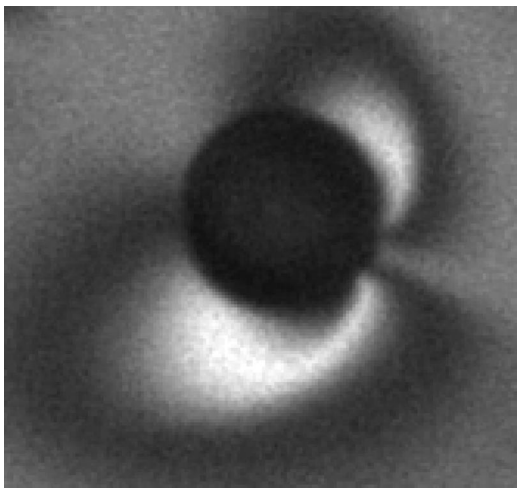

FIG. 7. Single droplet, SF20, diameter 41.5 μm, $T = 102\ ^\circ$C. Two $S = -1/2$ defects have formed to the right at the droplet border.

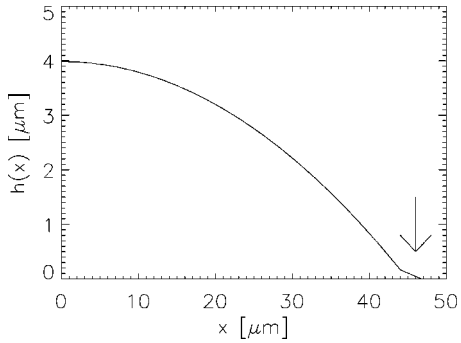

FIG. 8. Radial profile of a large droplet, extracted from the optical reflection image in monochromatic, unpolarized light. Note the "foot" of approximately 3 μm width (arrow position).

narrow regions of inhomogeneous film thickness, radial "wedges," in the smectic film around them. In earlier observations of other materials, where the droplets were generally much smaller, such regions have not been resolved. Optically it is not possible to determine the nature of these wedges. One possible explanation is the formation of terraces of excess smectic layers near the droplet. The excess energy necessary for the creation of the layer steps may be compensated by the reduction of film surface near the foot of the droplet. A typical profile determined optically is shown in Fig. 8.

Capillary forces are exerted by the film thickness gradient, and smaller droplets reaching the wedge are dragged into the big droplet. By this mechanism, big droplets absorb smaller droplets and grow. The width of the wedges depends on droplet size and temperature, it is commonly of the order of 10% of the droplet radius.

When the wedged region has formed around the droplet, the typical half integer defects of the director field disappear, they are replaced by inversion walls as seen in Fig. 9. These walls are always oriented in radial direction from the droplet, along the wedge gradient (Fig. 10). Within the walls, the *c* director rotates by 180° on a distance of a few microns. The film thickness steps (dislocations in the layer structure) tend

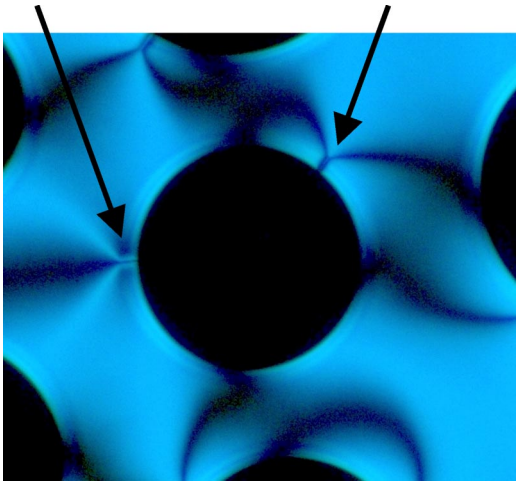

FIG. 9. (Color online) Droplet, SF20, diameter 50.0 μm, two walls, $T=101$ °C. The director orientation turns by 180° across the walls.

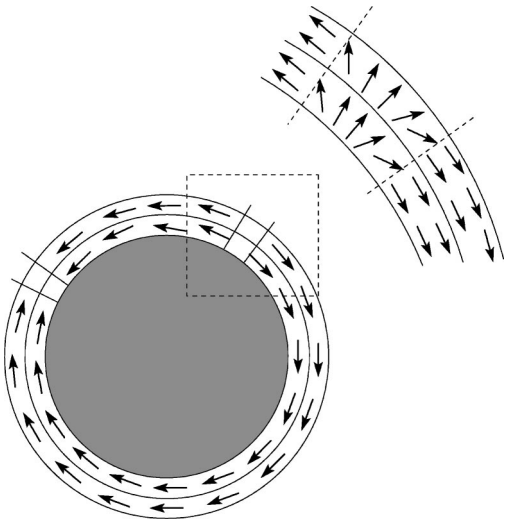

FIG. 10. Sketch of the director configuration and wall geometry in droplets with wedge interface, cf. the central droplet in Fig. 9. The inset is a magnification of the wall in the dashed rectangle.

to align the *c* director in a similar way as the smectic-isotropic interface. This prevents the director inversion from quenching into a point defect at the droplet border. We will analyze the wall geometry in the following subsection in more detail.

The number of walls attached to a single droplet can increase when the droplet absorbs a smaller droplet. Then it can inherit the walls/defects of the swallowed droplet. Huge droplets with four or more walls (necessarily always an even number) are found (see Fig. 11). However, another scenario is more common when two droplets coalesce, in particular when the radii of both droplets differ considerably. In that case, an inversion wall loop detaches from the small droplet and remains in the wedge region as is seen in Fig. 11. This leads to a growing number of loops collected in the wedge. The loops are stabilized by the same mechanism that stabilizes the straight radial inversion walls (see below).

We note that in huge droplets, we find also a characteristic structure inside the isotropic region (Fig. 11), which will not be analyzed here further.

C. Freezing of droplets

A way to prepare large regular wedges around the droplets is to cool the film rapidly after large isotropic droplets have formed. Upon cooling, part of the isotropic material in the droplet freezes into the smectic state again. If the excess smectic material cannot spread on the film fast enough, it forms additional layers on the film. Usually, this material is arranged around the droplets in the form of a radial wedge, again with a rather constant slope from the droplet towards the planar film. Figure 11 shows such a wedge around a droplet of 47.6 μm diameter that has been cooled from $T=102$ °C to $T=101$ °C at 90 °C per minute (setting of the heating stage). The measured slope, i.e., film thickness change per length, is of the order of 1:20 for most droplets (on average 50 nm distance between discrete single layer steps).

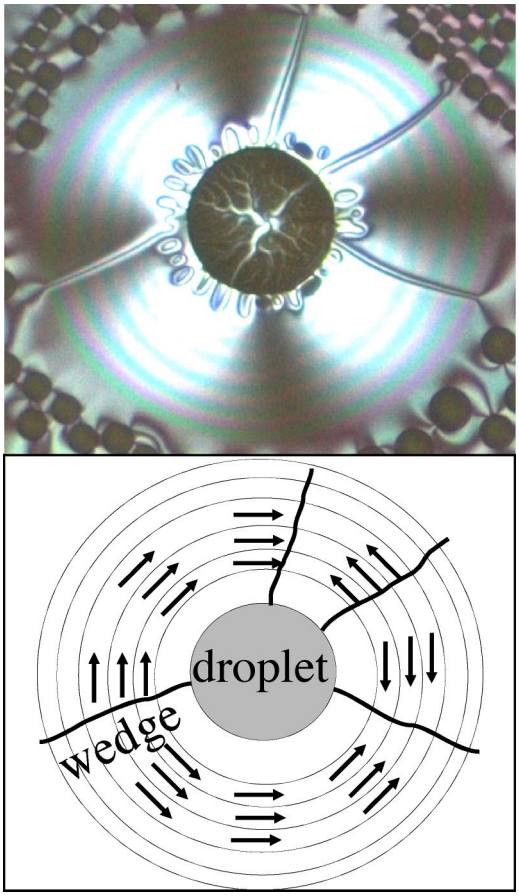

FIG. 11. (Color online) Partially frozen droplet of SF20, with a radial wedge and four inversion walls, prepared by rapid cooling from $T=102$ °C to $T=101$ °C, isotropic droplet diameter 47.6 μm, outer diameter of the wedge region 154 μm, the analyzer is rotated by 94° against the polarizer. In the bottom picture, arrows sketch the direction of the c director in the wedge.

As described above, the layer steps in the inhomogeneous film region impose a preferentially tangential alignment on the c director, and due to the competition of bulk deformation and anchoring conditions, the walls are not quenched to defects at the droplet border. They extend radially over the complete wedge, and they adopt a width that is given by the relation between the anchoring strength at the film thickness steps, the film thickness gradient, and elastic constants. The width of the inversion walls in Fig. 11 close to the droplet is ≈ 4 μm.

A model that describes the director field in the wedge can be constructed as follows: we assume that along the wedge gradient, the film has concentric rings of equidistant layer steps. When the individual steps are sufficiently close to each other, one can assume a director field as depicted in Fig. 12(a), i.e., independent of the coordinate y along the thickness gradient. The angle between the step and the c director is denoted by $\theta(x)$. We neglect the curvature of the layer steps in the vicinity of the wall, x is along the step. At the steps, the c director is anchored tangentially with a free energy contribution per area,

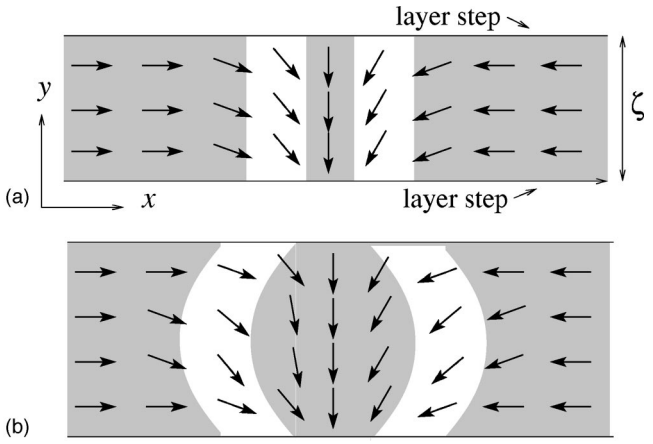

FIG. 12. Model of the c-director field in an inversion wall along the wedge gradient: (a) steep gradient, no director deformation along the gradient, (b) small gradient, complex two-dimensional deformation. The grey shade sketches the optical texture under crossed polarizers.

$$f_s = W_s(\vec{c}\cdot\vec{n})^2 = -W_s\cos^2\theta \tag{4}$$

(analogous to the anchoring at the smectic-isotropic interface) where W_s determines the strength of the coupling and $\vec{n}$ is the normal to the layer step. Using the elastic deformation energy expression, Eq. (1), in one constant approximation, the free energy per length element dx becomes

$$\mathrm{d}F = (f_e\zeta d + f_s d_l)\mathrm{d}x = \phi\mathrm{d}x \tag{5}$$

with the film thickness d, smectic layer thickness d_1, and the distance of neighboring layer steps ζ. The anchoring free energy of each layer step contributes with factor $1/2$ on the c director on each side, and one has to consider two layer steps per segment. The equilibrium wall profile follows from the Euler-Lagrange equation:

$$\frac{1}{2}Kd\zeta(\theta')^2 - W_s d_l\cos^2\theta = \text{const}$$

($\theta' = d\theta/dx$). Solutions with the correct boundary conditions are

$$\theta(x) = 2\arctan\left[\exp\left(\pm\frac{x}{\xi_s}\right)\right] \tag{6}$$

with

$$\xi_s = \sqrt{\frac{Kd\zeta}{2W_s d_l}}.$$

The optical appearance of such a wall profile is in good agreement with the experimental observations; a fit of the width ξ_s can be used to estimate W_s. With an average slope $d_1/\zeta \approx 1/20$, a film thickness d of approximately 300 nm, and the experimental value $\xi_s \approx 1$ μm (roughly $1/4$ of the wall width), we obtain a ratio K/W_s in the order of magnitude of 1.4 μm.

When the distance between parallel layer steps becomes larger, the c director chooses a compromise between the wall width and the deformation in the area between the steps; the

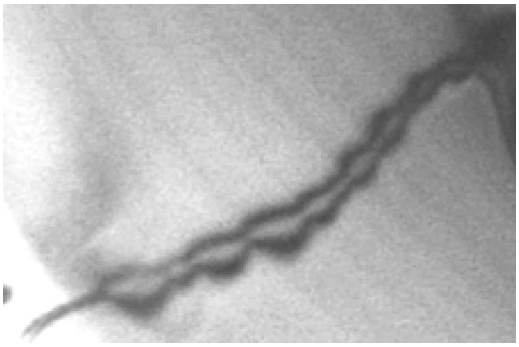

FIG. 13. Detail of an inversion wall in a film region with weak thickness gradient [cf. Fig. 12(b)].

resulting *c*-director configuration between two steps and the resulting optical texture are sketched in Fig. 12(b). An experimental example is seen in Fig. 13.

D. Droplet interactions and self-organization

The droplets do not remain randomly distributed on the film but attract each other, in regions of uniform film thickness, via the director field. As already discussed in the model subsection, sufficiently *small* droplets can exist in a defect-free *c*-director environment. When two such droplets approach each other, they can share the induced deformation, thus lowering the elastic free energy [Fig. 5(a)]. This situation is in principle comparable to that reported in Ref. [13] for nematic droplets. Note, however, that Cluzeau *et al.* interpret their *c*-director configuration as similar to that shown in Fig. 3(b) above. In contrast, we find by a close inspection of the surroundings of the individual droplets that the director field is defect free [Fig. 3(a)]. Instead, the anchoring conditions on the isotropic droplet surface are not strictly tangential because of the relatively weak anchoring strength for the *c* director. The question of whether this is a peculiarity of isotropic droplets or whether an accurate exploration would reveal similar deviations from strict planar anchoring at the nematic droplet boundaries has yet to be solved. Droplets embedded in a uniform director field line up in a direction roughly diagonal to the undistorted director [arrows in Figs. 14(a) and 14(b)]. Within our model, and in accordance with the interpretation of nematic droplet arrays in Ref. [13], this is a consequence of the quadrupolar character of the induced deformation, where all four diagonal positions of the second droplet with respect to the first one in the pair are energetically equivalent. A few minutes after their formation, no isolated droplets are observed any more, they have organized in groups of droplets. An example of chaining of droplets in a defect-free environment is shown in Fig. 14(b). Note that the embedding undistorted director orientation is nearly diagonal to the chain axes.

For droplets that carry a pair of $S=-1/2$ surface defects [the type shown in Figs. 3(c) and 7], the situation is qualitatively different. When two such droplets approach each other, they start to reorient due to their mutual interaction, similar to electrical dipoles (and similar to $S=\pm 1$ topological charge pairs [16]), until the defect pairs point into the same

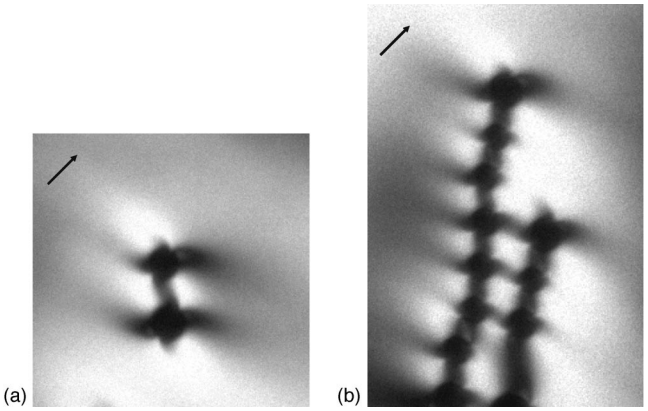

FIG. 14. (a) Interaction of two droplets in an SF20 film, diameter of droplets 5.0 μm, $T=97.5$ °C. (b) Two droplet chains, SF20, diameter of droplets ≈ 3.9 μm, $T=89.5$ °C. The *c*-director field is defect free in both images, and the interactions are of a quadrupolar type.

direction, parallel to the droplet interconnection vector. The two droplets approach until they reach a distance which is essentially given by their radius. We have measured the distance D between centers of neighboring droplets as a function of their average diameter in a temperature range between $T=89.5$ °C and $T=106.5$ °C. As expected, a linear relation fits the data in the presented experimental range (Fig. 15), no significant temperature dependence was found. The slope of this linear fit is 1.28. This value is roughly the same as that obtained for cholesteric droplets in Sm-C^* films [10,15] where the authors have analyzed chains in which the droplets were separated by isolated $S=-1$ defects in the *c*-director field.

The assembly of further droplets leads to the formation of chains, in which each droplet carries two half integer surface defects aligned in the same direction. The experimental observation is shown in Fig. 16(a), while Fig. 16(b) sketches the director field in such a chain. The director orientation far from the droplet differs significantly from the case discussed above. Here, the symmetry axis of the embedding director field is along the long axis of the pair, the *c* director at both sides of the chain is deflected towards an antiparallel orien-

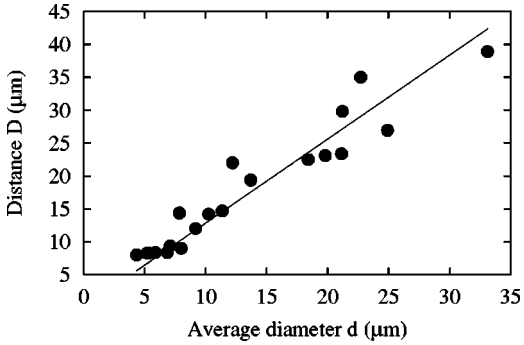

FIG. 15. Plot of the equilibrium distance D between droplets centers as a function of their average diameter $d=2r$. The temperature ranges between $T=89.5$ °C and $T=106.5$ °C. The films are roughly 100 layers thick, a film thickness dependence of the equilibrium distances has not been considered here.

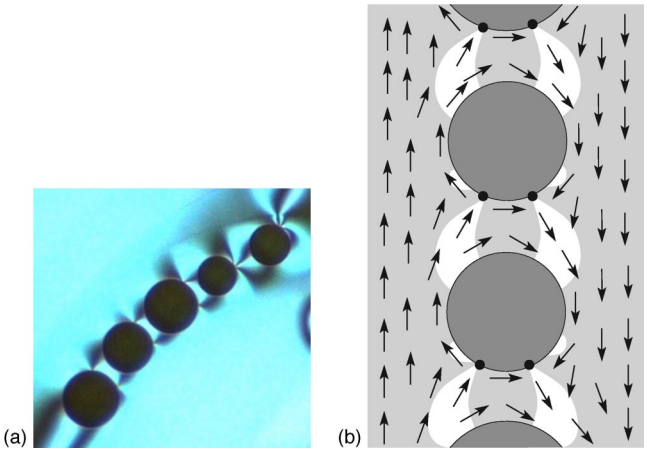

FIG. 16. (Color online) (a) Formation of a droplet chain, SF20, diameter of bottom droplet 24.9 μm, two defects per droplet, $T=101\,^{\circ}$C, and the corresponding director field. (b) The shades in the schematic director field presentation sketch the optical texture for crossed polarizers along and perpendicular to the chain.

tation. When the chain is long enough, the *c*-director orientation on both sides of the chain becomes antiparallel, in the direction of the chain axis.

An impressive demonstration of the interactions between droplet chains and director field could be found in the photosensitive material 11OAB. Here, the anchoring properties of the droplets are the same as in SF20, although the droplets are much smaller in size. Induction of droplets can be controlled in this material by the intensity of light illumination on the sample. The azoxy group performs a photoisomerization from the *trans* into the *cis* configuration, which leads to the destruction of the local smectic order and a certain reduction of the clearing temperature with increasing intensity of incident light.

In an 11OAB film in the Sm-*C* phase, we have prepared a periodic pattern consisting of a continuously distorted director field. Such patterns can be prepared, e.g., by mechanical rotation of the film [24], by rotating electromagnetic fields [25–27], or by electrically or thermally driven convection [28–30]. In absence of droplets, its optical appearance is that of a target pattern of dark and bright rings around the film center. Far from the center, it corresponds to a *c*-director field with an approximately constant radial gradient of the azimuthal angle θ. Figure 17(a) shows an example of a continuously distorted director field. The slight difference between neighboring stripes in the image is due to the elastic anisotropy, indeed the splay elastic constant K_S of 11OAB is somewhat larger than the bend constant K_B. This pattern is perfectly suited to study the arrangement of droplets in a periodically deformed director field and the interaction between droplet chains and *c*-director field. In this periodic structure, all the droplets are gathered in chains, which are aligned along isoclines of the original *c*-director pattern. It is obvious from Fig. 17(b) that the chains prefer the regions where the *c* director points in the direction of the director gradient (bend regions), and that they contract these regions because of the anchoring conditions at the droplet interface. The original *c*-director structure is seen in the few places

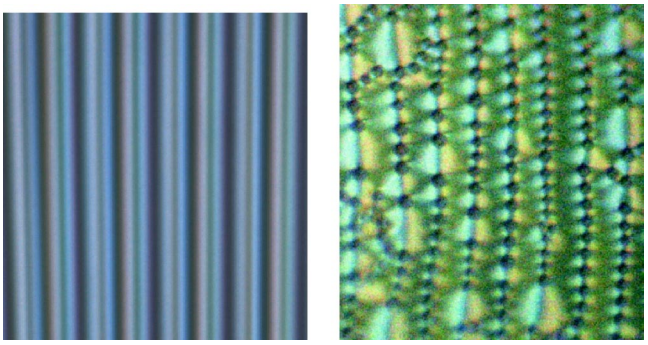

FIG. 17. (Color online) (a) Continuously rotated director field in absence of droplets (at $T=118\,^{\circ}$C and low illumination) and (b) droplet chains of 11OAB aligned by the externally imposed *c*-director pattern, the width of the image is 107 μm, $T=122\,^{\circ}$C.

where chains are interrupted. The *c*-director field in the vicinity of the droplets is that of Fig. 16(b). It is obvious here that the droplet chains separate regions of exactly opposite *c*-director orientations, parallel and antiparallel to the chain axis. The droplets in this material have a very narrow size distribution. As in SF20, the interdroplet distance in the chains is well defined, it is given by the droplet size and the equilibrium configuration of the director deformation in the chain. Because of the very small droplet size, it is not as easy as in SF20 to resolve the detailed defect structure in the chains optically, but qualitatively the same model of the director configuration applies.

E. Lattices

When the density of droplets becomes very high, they start to form lattices. Preliminary investigations show that depending on the droplet density and type of director configurations, different lattice types can be observed.

Figure 18 shows an arrangement of droplets in an 11OAB film. They form a hexagonal lattice, which is best seen by the two-dimensional Fourier transform of the optical image.

V. CONCLUSIONS

The self-organization of isotropic droplets in smectic-*C* free-standing films has been investigated. The films have

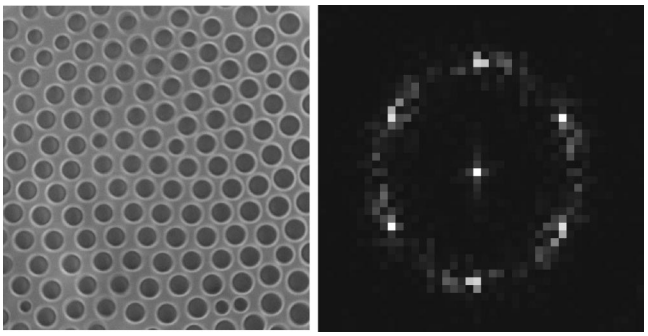

FIG. 18. Left: Hexagonal lattice formed by isotropic droplets in 11OAB, average droplet diameter 17.5 μm, no analyzer, $T=122\,^{\circ}$C; right: two-dimensional Fourier transform of the texture of the hexagonal pattern, the wave number of the six reflexes is 0.28 μm^{-1}.

been heated to the transition from the Sm-*C* phase to the isotropic phase. In the vicinity of the bulk transition temperatures, one observes the formation of micrometer droplets in the film plane. A characteristic feature of the droplets in the Sm-*C* films is their mutual interaction by elastic distortions of the *c*-director field. While the self-organized structures found in this study are very similar to those reported for cholesteric droplets in Sm-*C** films, we have demonstrated that the *c*-director field in detail is very different from that reported in Ref. [10]. In particular, the investigation of the director configurations in the vicinity of large droplets reveal many details of the induced deformations, symmetries, and mechanisms of spontaneous self-organization. We do not find isolated defects near the droplets but instead, defect-free configurations or defect pairs on the droplet boundaries. On the basis of these qualitative observations, and the detailed analysis of the deformation structures, it will be possible to calculate quantitative interaction forces and to derive anchoring energies and elastic constants of the material in numerical simulations.

The question why isolated defects of strength −1 are absent in the system studied here can be answered only speculatively. It is established in our systems that the droplet generation and growth in an initially defect-free *c*-director field necessarily leads to bound half integer defects. In that respect, there is no principle difference to the chiral smectic phase studied, e.g., in Ref. [16]. Assuming that the interpretation of the director textures is correct there, one is forced to conclude that the nematic (or *N**) to smectic interface, which is probably less sharp than the isotropic-smectic interface due to fluctuations of smectic layer order, is involved in the detachment process. In that case, the isotropic droplets would represent a more appropriate model system for other isotropic inclusions (water, oil) in smectic free-standing films.

Finally, we have shown that it seems possible to structure the droplet arrangement by a specially prepared director pattern, and to use the interactions of droplets with structured director fields to create regular droplet micropatterns.

ACKNOWLEDGMENTS

It is a pleasure to thank Alexej Eremin, Peter Karich, Heidrun Schüring, and particularly Philipe Cluzeau for valuable discussions. The authors are much indebted to Wolfgang Weissflog and Sonja Findeisen for the supply of the mesogenic material.

[1] P.S. Drzaic, *Liquid Crystal Dispersions* (World Scientific, Singapore, 1995), Vol. 1.
[2] P. Poulin, H. Stark, T.C. Lubensky, and D.A. Weitz, Science **275**, 1770 (1997).
[3] P. Poulin, V. Cabuil, and D.A. Weitz, Phys. Rev. Lett. **79**, 4862 (1997).
[4] P. Poulin and D.A. Weitz, Phys. Rev. E **57**, 626 (1998).
[5] H. Schüring and R. Stannarius, Langmuir **18**, 9735 (2002).
[6] H. Schüring and R. Stannarius, Mol. Cryst. Liq. Cryst. **412**, 2035 (2004).
[7] H. Schüring and R. Stannarius, in *Molecules in Interaction with Surfaces and Interfaces*, Lecture Notes in Physics Vol. 634, edited by R. Haberland, D. Michel, A. Pöppl, and R. Stannarius (Springer, New York, 2004), p. 337.
[8] R. Najjar, Y. Galerne, Mol. Cryst. Liq. Cryst. Sci. Technol., Sect. A **367**, 475 (2001).
[9] V.K. Dolganov, E.I. Demikhov, I. Fouret, and C. Gors, Phys. Lett. B **220**, 242 (1996).
[10] P. Cluzeau, P. Poulin, G. Joly, and H.T. Nguyen, Phys. Rev. E **63**, 031702 (2001).
[11] P. Cluzeau, V. Dolganov, P. Poulin, G. Joly, and H.T. Nguyen, Mol. Cryst. Liq. Cryst. Sci. Technol., Sect. A **364**, 381 (2001).
[12] P.V. Dolganov, E.I. Demikhov, V.K. Dolganov, B.M. Bolotin, and K. Krohn, Eur. Phys. J. E **12**, 593 (2003).
[13] P. Cluzeau, G. Joly, H.T. Nguyen, and V.K. Dolganov, Pis'ma Zh. Eksp. Teor. Fiz. **75**, 573 (2002) [JETP Lett. **75**, 482 (2002)].
[14] P. Cluzeau, G. Joly, H.T. Nguyen, and V.K. Dolganov, Pis'ma Zh. Eksp. Teor. Fiz. **76**, 411 (2002) [JETP Lett. **76**, 351 (2002)].
[15] P. Cluzeau, V. Bonnand, G. Joly, V. Dolganov, and H.T. Nguyen, Eur. Phys. J. E **10**, 231 (2003).
[16] P. Cluzeau, F. Bougrioua, G. Joly, L. Lejček, and H.T. Nguyen, Liq. Cryst. **31**, 719 (2004).
[17] H. Stark, Phys. Rep. **351**, 387 (2001), and references therein.
[18] T.C. Lubensky, D. Pettey, N. Currier, and H. Stark, Phys. Rev. E **57**, 610 (1998).
[19] J. Fukuda, H. Stark, M. Yoneya, and H. Yokoyama, Phys. Rev. E **69**, 041706 (2004).
[20] P.S. Pershan, *Structure of Liquid Crystal Phases* (World Scientific, Singapore, 1988).
[21] D. Pettey, T.C. Lubensky, and D. Link, Liq. Cryst. **25**, 579 (1998).
[22] S.A. Langer and J.P. Sethna, Phys. Rev. A **34**, 5035 (1986).
[23] I. Kraus and R.B. Meyer, Phys. Rev. Lett. **82**, 3815 (1999).
[24] P.E. Cladis, Y. Couder, and H.R. Brand, Phys. Rev. Lett. **55**, 2945 (1985).
[25] P.E. Cladis, P.L. Finn, and H.R. Brand, Phys. Rev. Lett. **75**, 1518 (1995).
[26] G. Hauck and H.D. Koswin, Ferroelectrics **122**, 253 (1995).
[27] R. Stannarius, Ch. Langer, and W. Weißflog, Phys. Rev. E **66**, 031709 (2002).
[28] S.W. Morris, J.R. de Bruyn, and A.D. May, Phys. Rev. Lett. **65**, 2378 (1990).
[29] A. Becker, S. Ried, R. Stannarius, and H. Stegemeyer, Europhys. Lett. **39**, 257 (1997).
[30] M.I. Godfrey and D.H. van Winkle, Phys. Rev. E **54**, 3752 (1996).